Photodissociation of $I_2^-(OCS)_n$ Cluster Ions: Structural Implications

S. Nandi, A. Sanov, N. Delaney, J. Faeder, R. Parson, and W. C. Lineberger*

JILA, National Institute of Standards and Technology and University of Colorado, and Department of Chemistry and Biochemistry, University of Colorado, Boulder, Colorado 80309-0440

Received: June 29, 1998; In Final Form: September 2, 1998

We report product distributions from the photodissociation of $I_2^-(OCS)_n$ ($n = 1-26$) cluster ions at 790 and 395 nm and discuss implications concerning the structure of these clusters. The experimental results are paralleled by a theoretical investigation of $I_2^-(OCS)_n$ structures. The 790 and 395 nm transitions in I_2^- access dissociative excited states that correlate with the $I^- + I(^2P_{3/2})$ and $I^- + I^*(^2P_{1/2})$ products, respectively. Photoabsorption by $I_2^-(OCS)_n$ clusters at 790 nm results in "uncaged" $I^-(OCS)_k$ and "caged" $I_2^-(OCS)_k$ fragments. The 395 nm excitation leads, in general, to three distinct pathways: (1) I_2^- dissociation on the $I^- + I^*(^2P_{1/2})$ spin−orbit excited asymptote, competing with the solvent-induced spin−orbit relaxation of $I^*(^2P_{1/2})$ followed by either (2) I_2^- dissociation on the $I^- + I(^2P_{3/2})$ asymptote or (3) I_2^- recombination. Pathways 1 and 2 result in a bimodal distribution of the uncaged $I^-(OCS)_k$ fragments that energetically correlate with the two spin−orbit states of the escaping I atom. The $I + I^-$ caging efficiency is determined as a function of the number of solvent OCS molecules at both excitation wavelengths studied. At 790 nm, 100% caging of I_2^- is achieved for $n \geq 17$. For 395 nm excitation, addition of the 17th OCS molecule to $I_2^-(OCS)_{16}$ results in a steplike increase in the caging efficiency from 0.25 to 0.68. These results suggest that the first solvent shell around I_2^- is comprised of 17 OCS molecules. Results of theoretical calculations of the lowest-energy $I_2^-(OCS)_n$ cluster structures support this conclusion. The roles of different dominant electrostatic moments of OCS and CO_2 in defining the $I_2^-(OCS)_n$ and $I_2^-(CO_2)_n$ cluster structures are discussed, based on comparison of the photofragment distributions.

I. Introduction

The dramatic effects of solvation on the outcomes and rates of chemical reactions have motivated many experimental and theoretical studies of reactions in solutions and clusters. A topic of particular interest is the solvent-induced recombination, or "caging" of photofragments.[1−25] While many groups have studied caging in high-pressure gases, matrices, and liquids, the microscopic details of the reaction in these environments are often obscured by the multitude of local solvent configurations and inherent inability of resolving separate product channels. Our group has emphasized the gas-phase dynamics of dihalogen anion recombination in various size-selected clusters.[26−33] The cluster-ion approach allows the capability not only to select (and systematically vary!) the initial solvation conditions but also to mass analyze the final ionic products.[34] In this respect, clusters offer a unique, well-characterized and controlled environment for studies of solvation and intermolecular interactions.[34−37]

The photodissociation of I_2^- presents an important model case. The electronic structure of I_2^- is represented by six doubly degenerate electronic states lying energetically lower than the ground state of neutral I_2.[38,39] The scaled potential energy curves corresponding to the ionic states are shown in Figure 1.[40−42] The ground state of I_2^- has a well depth of 1.01 eV[39,43] and in a simple molecular orbital picture corresponds to a bond order of $^1/_2$. Upon solvation, the charge of I_2^- leads to relatively strong electrostatic interactions with adjacent solvent molecules, while the weakness of the bond allows the solvent to dramatically perturb the electronic structure of the ion.[38,44]

In addition to the studies of I_2^- recombination dynamics in liquid water and alcohols by Barbara and co-workers,[20−22] our group has extensively studied the caging of I_2^- in clusters following photodissociation in the visible−near-IR wavelength range.[26−30,32,33,45−47] Kondow and co-workers examined collisions of $I_2^-(CO_2)_n$ cluster ions with solid surfaces and observed the wedge effect: the solvent CO_2 molecules sandwiched between the surface and the I_2^- waist in a collision split the I_2^- bond.[48−51] Several recent studies provided theoretical background for understanding the dissociation and recombination

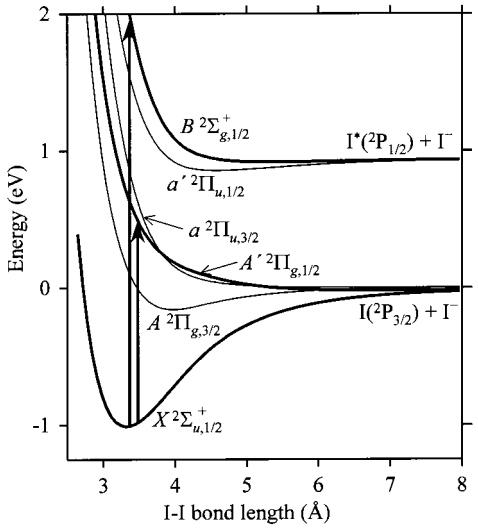

Figure 1. I_2^- potentials calculated by Faeder et al.[38] The ab initio potentials have been scaled[38] to match the experimental I_2^- well depth.[25,39] Arrows indicate the transitions studied in this work. The upper and lower case prefixes in the electronic state labels correspond to allowed and forbidden optical transitions from the ground (X) state, respectively.

10.1021/jp982794y CCC: $15.00 © 1998 American Chemical Society
Published on Web 10/14/1998

processes.[9,11,38,52−54] Parson and co-workers examined I_2^- embedded in various clusters[11,38,54] and described this system in terms of an intramolecular Marcus theory[55,56] framework. In their analysis, the photofragmentation and caging processes are mediated by the coupling of electronic states with differential charge character that is caused by the interaction with the solvent.[11,38,54] They have shown that differential solvation of electronic states can lead to isoenergetic curve-crossing regions.

In this paper, we report the photodissociation and caging of I_2^- in OCS clusters. This work complements our studies of I_2^- in CO_2,[26−28,32,33,45] N_2O,[30] and Ar[28,29] clusters, allowing for a comparison of the effects of isovalent solvents with differing electrostatic properties on the dissociation and recombination dynamics. In all previous studies, the $A'\,^2\Pi_{g,1/2} \leftarrow X\,^2\Sigma^+_{u,1/2}$ transition centered near 750 nm[27,40,42] was utilized to promote the photodissociation of I_2^-, yielding the $I^- + I(^2P_{3/2})$ products. Here, the same electronic transition, indicated by an arrow in Figure 1, is employed to induce the photodissociation and caging of I_2^- embedded in the OCS solvent. Additionally, we utilize 395 nm photodissociation of $I_2^-(OCS)_n$, whereby I_2^- is excited via the $B\,^2\Sigma^+_{g,1/2} \leftarrow X\,^2\Sigma^+_{u,1/2}$ transition[40,57,58] to a repulsive state correlating with the $I^- + I^*(^2P_{1/2})$ dissociation limit, as also shown in Figure 1. Our measurement of the translational energy release in 395 nm photodissociation of bare I_2^- indicates exclusive production of the $I^- + I^*(^2P_{1/2})$ products. Within a cluster, however, solvent-induced spin−orbit relaxation is possible, resulting in three distinct reaction pathways including the dissociation on both $I^- + I(^2P_{1/2,3/2})$ asymptotes, as well as the recombination (caging) of the I_2^- chromophore. Competition between the three near-UV fragmentation channels provides a delicate probe of the solvent-induced couplings between different electronic states of I_2^-.

The organization of this paper is as follows. Section II describes the theoretical simulations of the $I_2^-(OCS)_n$ cluster structures. A brief description of the cluster ion source and the tandem time-of-flight mass spectrometer apparatus is given in section III. In section IV the results of photofragmentation experiments on $I_2^-(OCS)_n$ at 790 and 395 nm are presented. Section V presents a discussion of the dissociation and caging dynamics with an emphasis on the structural implications for the $I_2^-(OCS)_n$ cluster ions. Section VI contains a summary of results and conclusions.

II. Structure of $I_2^-(OCS)_n$ Cluster Ions

Electrostatic interactions of the charged cluster core with OCS are dominated by the charge−dipole (μ(OCS) ≈ 0.7 D)[59] interaction. This is in contrast with the $I_2^-(CO_2)_n$ clusters, where the absence of a permanent dipole moment and the 5 times larger quadrupole moment of CO_2 imply that the charge−quadrupole interaction determines the cluster structure.[60−62] Additionally, the fact that carbon dioxide forms dry ice, while carbonyl sulfide does not, implies weaker interaction within the OCS solvent shell itself, compared to the case of the CO_2 shell.

Since the charge in I_2^- is equally partitioned between the two I atoms, a single OCS molecule is expected to bind near the waist of I_2^- with the positively charged S atom pointing toward the I_2^- center of mass. In larger $I_2^-(OCS)_n$ clusters, solvent−solvent interactions must be taken into account. In the limit of weak solvent−solvent interactions, they could be considered as a perturbation to the solute−solvent binding. In this approach, the dominant solvent binding to the cluster core orients neighboring OCS molecules in a complete solvent shell nearly parallel to each other, causing dipole−dipole repulsion, which is estimated to be ∼1 eV at a separation of 2.4 Å.[63,64] On the other hand, the theoretical study of Bone revealed a number of bound $(OCS)_2$ van der Waals structures with binding energies of as much as 78 meV.[65] These large binding energies suggest that solvent−solvent interactions can contribute constructively to the average energy of solvent binding to the cluster.

We therefore expect the solvent in the smallest $I_2^-(OCS)_n$ clusters to be bound around the chromophore in a charge−dipole orientation, with the sulfur ends pointing toward the waist of I_2^-. As the number of solvent molecules increases, the most energetically favorable structures must accommodate both the solvent−solute and solvent−solvent interactions. We begin the quantitative analysis of the $I_2^-(OCS)_n$ structures by examining the interaction within the $I^-(OCS)$ complex using the first-principles theoretical methods. The analysis is then extended to the $I_2^-(OCS)$ complex. Finally, we incorporate these results into an effective Hamiltonian treatment of the structure of larger clusters.

A. First-Principles Characterization of the $I^-\cdots$OCS and $I_2^-\cdots$OCS Interactions. The first-principles calculations were carried out with Gaussian 94[66] using spin-restricted Becke's three-parameter, hybrid density functional method[67] with the correlation functional of Lee, Yang, and Parr[68] (B3LYP). The basis set used for iodine was based on the effective core pseudopotential (ECP) developed by Hay and Wadt[69] combined with a double-ζ valence basis set (LanL2DZ). Following the recommendation of Glukhovtsev, Pross, and Radom,[70] we added uncontracted s and p diffuse functions (exponents 0.0569 and 0.0330, respectively) and d and f polarization functions (exponents 0.292 and 0.441, respectively). As for OCS, special attention was paid to the adequate description of its electrostatic properties. For the O, C, and S centers, we employed the all-electron correlation consistent aug-cc-pVDZ basis sets of Dunning,[71−73] which at the B3LYP level of theory resulted in a calculated OCS dipole moment of 0.73 D, consistent with the experiment.[59]

The $I^-(OCS)$ complex has a linear $I^-\cdots$SCO global minimum structure. A small bend in OCS is expected at the nonlinear geometries. However, the effect of the OCS bend is not significant (see below), and most of the calculations were carried out for rigid OCS frozen at the optimized linear geometry of the isolated molecule. This simplification allowed us to take advantage of cylindrical symmetry, reducing the problem to two coordinates: the distance R from the OCS center of mass to I^- and the angle θ between the SCO and **R** vectors ($\theta = 180°$ corresponds to the linear $I^-\cdots$SCO structure).

Figure 2 shows the calculated potential energy surface (PES) for the interaction of rigid OCS with I^-. The numerical data describing this surface can be found on-line in the Supporting Information to this paper. The features of the $I^-(OCS)$ PES agree well with intuitive expectations. The global potential minimum corresponds to the linear $I^-\cdots$SCO charge−dipole bound geometry with an S−I distance of 3.6 Å and a dissociation energy of 220 meV. The secondary charge−quadrupole interaction results in a shelflike region of the PES near the T-shaped geometry ($\theta \approx 90°$) characteristic of the charge−quadrupole bound complexes such as $I^-(CO_2)$[74−76] and $I^-(N_2O)$.[74] The interaction energy in this shelflike region was calculated to be about 67 meV, and the "barrier" separating this region of the PES from the charge−dipole global minimum at $\theta = 0°$ was found to be negligibly small (∼1 meV).

Similar calculations[76] on $I^-(CO_2)$ predicted a T-shaped (C_{2v}) equilibrium geometry of the complex, characterized by an I−C distance of 3.65 Å and an OCO bend of 174.3°. The adiabatic

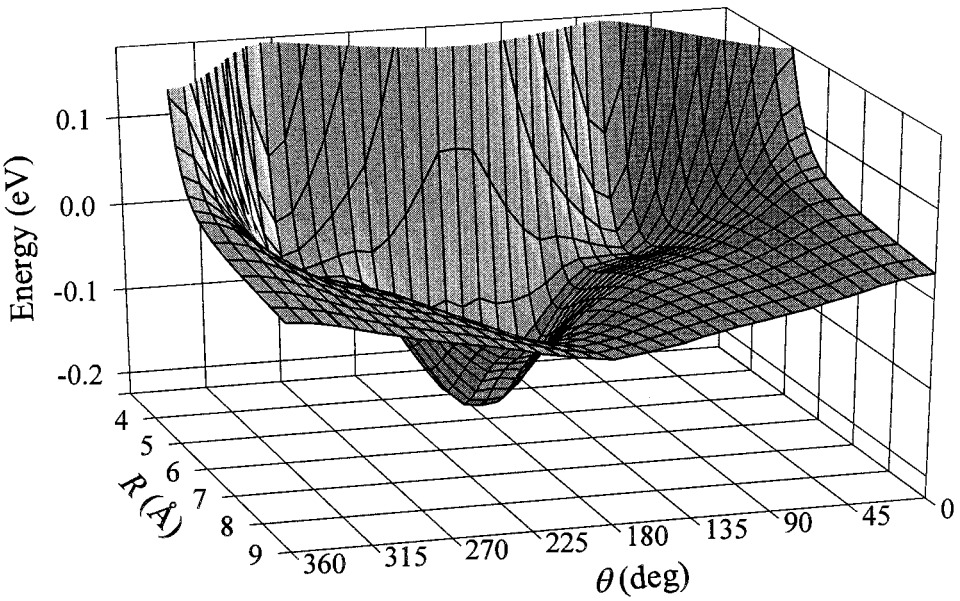

Figure 2. $I^-\cdots SCO$ potential energy surface calculated using the spin-restricted B3LYP method. OCS is frozen at its linear equilibrium geometry. The zero of energy corresponds to I^- and OCS at infinite separation. R is the distance from the OCS center of mass to I^-; θ is the angle between the **R** vector and the SCO axis ($\theta = 180°$ corresponds to the linear $I^-\cdots SCO$ geometry). Color version of this figure (Figure 2S) and the numerical data for the potential energy surface can be found on-line in the Supporting Information section of the Web edition of this publication.

binding energy of CO_2 to I^- is calculated to be 149 meV. However, the *vertical* electron detachment energy (VDE) of $I^-(CO_2)$ is calculated to be larger than the electron detachment energy of bare I^- by 175 meV. This is in excellent agreement with the 172 meV shift in the photoelectron spectrum of $I^-(CO_2)$ relative to that of bare I^-, observed by Neumark and coworkers.[74] The substantial difference between the $I^-(CO_2)$ complex binding energy and its VDE is due to the significant OCO bend within the complex. To the contrary, the effect of OCS bending in the T-shaped configuration of the $I^-(OCS)$ complex is predicted to be much smaller. Relaxing the OCS bending angle near $\theta \approx 90°$ leads to additional stabilization of just ~1 meV at an optimized OCS bending angle of 178°. The bending of OCS is nullified at the linear equilibrium geometry of the $I^-(OCS)$ complex. Therefore, electron transfer from the anion to the solvent appears to be unimportant in $I^-(OCS)$.

Selective calculations on the $I_2^-(OCS)$ complex indicated that the interaction of OCS with I_2^- is qualitatively similar to that in $I^-(OCS)$, dominated by the charge−dipole interaction. The most favorable binding site for OCS corresponds to the T-shaped (C_{2v}) structure bound by 137 meV, with the S end of OCS pointing toward the waist of I_2^- and an S−I_2^- center-of-mass distance of 3.7 Å. The $I_2^-(OCS)$ PES was found to be nearly flat with respect to small shifts in the position of OCS along the I_2^- bond, as the I_2^- and OCS axes were kept perpendicular. The calculated binding energy of the linear $(I-I)^-\cdots SCO$ structure at an optimized S−I distance of 3.8 Å is 114 meV.

B. Model Hamiltonian Determination of the $I_2^-(OCS)_n$ Cluster Structures. For larger $I_2^-(OCS)_n$ clusters, the energetically favorable structures must accommodate both the solvent−solute and solvent−solvent interactions. We employ methods developed by Faeder et al.[77−79] to study the structures of larger clusters. The publication of full details of the simulation of the $I_2^-(OCS)_n$ structures will be forthcoming; in this paper, we give only a brief qualitative description of the technique and present a few preliminary results.

The Hamiltonian for the interaction between the solute and solvent is a sum of long-range electrostatic and polarization terms and short-range dispersion and repulsion interactions. We use this Hamiltonian, with the parameters defined below, to run molecular dynamics simulations on the ground electronic state of the solute with cycles of heating and cooling followed by a quasi-Newton optimization to determine the structures of I_2^- clustered to up to 17 OCS molecules. The solvent electrostatics are represented by point charges placed along the internuclear axis. The polarizability of OCS is represented by a single site at the center of mass with different polarizabilities parallel and perpendicular to the internuclear axis. In ionic systems, we expect the long-range interactions to dominate the interaction potential; we therefore approximate the short-range interactions with state-independent atom−atom Lennard-Jones potentials.

Electron transfer from I_2^- to the solvent was not allowed in the electrostatic model. The validity of this assumption is corroborated by the ab initio calculations on $I^-(OCS)$ and $I_2^-(OCS)$ in section II.A. We assign a three-point charge model for OCS by solving a system of linear equations for the charge, dipole, and quadrupole moments of OCS, which are 0, 0.7152 D, and −0.79 D Å, respectively.[80] The resulting charges on the O, C, and S atoms are −0.0766, 0.0382, and 0.0385 au, respectively. We note that this is an overly simple method for selecting point charges, and we do not expect it to accurately describe the OCS charge distribution. The molecular polarizability, $\alpha = 5.21$ Å^3, and the polarizability anisotropy, $\gamma = 4.67$ Å^3,[80] were used to determine the parallel and perpendicular polarizabilities of 8.32 and 3.65 Å^3, respectively.

The short-range interactions are accounted for with atom−atom Lennard-Jones potentials. Parameters for OCS···OCS interactions were taken from simulations of liquid OCS.[81] The I···S parameters were chosen so that the total interaction potential of I···OCS reproduces the geometry and energy of the dipole bound minimum of the ab initio calculation described above. The I···O and I···C parameters were selected to create a repulsive potential as I^- approaches the O end of OCS and to match the ab initio energy of the T-shaped configuration. While the resulting model potential for the $I^-\cdots OCS$ complex qualitatively agrees with main features of the ab initio potential shown in Figure 2, some differences between the two potentials (to be discussed in a future publication) dictate caution in

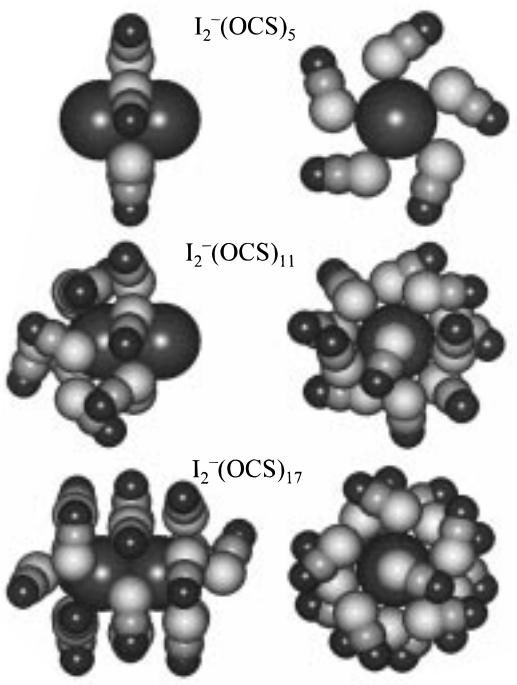

Figure 3. Calculated minimum-energy structures of $I_2^-(OCS)_n$, n = 5, 11, and 17. The two columns show the same structures as viewed along the axes perpendicular (left) and parallel (right) to the I_2^- bond. Structures shown correspond to selected isomers out of many nearly isoenergetic solvent configurations. While the general manner of solvent packing about the I_2^- (five-membered ring formation) is reproduced in all low-energy isomers, local structural details, such as the relative orientation of neighboring OCS molecules, may vary. Color version of this figure (Figure 3S) can be found on-line in the Supporting Information section of the Web edition of this publication.

interpreting the quantitative parameters of the $I_2^-(OCS)_n$ structures reported here. In particular, bending about the linear $I^-\cdots SCO$ minimum is too facile in the model potential. Additionally, the binding energy of the C_{2v} $I_2^-(OCS)$ structure predicted by the model is 230 meV, considerably larger than determined from the electronic structure calculation. Parametrizing the $I_2^-\cdots SCO$ interaction potential is difficult because very little is known about either the potential itself or the interactions among the various fragments. To the best of our knowledge, the ab initio calculations presented above represent all that is known about the $I^-\cdots SCO$ potential.

Using this model to determine minimum-energy structures of $I_2^-(OCS)_n$, some of which are shown in Figure 3, we find that OCS molecules arrange themselves first about the waist of I_2^- with the sulfur atoms, nearest the solute, about 3.6 Å from the I_2^- center of mass. The solvent molecules are tilted at about 117° toward one another, rather than pointing radially outward, as seen in the $I_2^-(OCS)_5$ structure in Figure 3. In the $I_2^-(OCS)_5$ cluster ion, five OCS molecules complete a ring around I_2^-. Additional OCS molecules form a second ring around one end of the solute, and then a single OCS molecule fills the axial site, completing the half-shell $I_2^-(OCS)_{11}$ structure shown in Figure 3. The other side is filled in the same fashion, completing the first solvent shell at $n = 17$.

In contrast, for $I_2^-(CO_2)_n$ clusters the dominant charge−quadrupole interactions result in CO_2 molecules lying flat with respect to I_2^-. Using a similar model,[38,77] we have shown that in small clusters CO_2 molecules pack together on one side of the I_2^- core rather than forming a ring,[11,60] as shown in Figure 4 for $I_2^-(CO_2)_5$ (compare to the $I_2^-(OCS)_5$ structure in Figure 3). The packing of CO_2 tends to increase the number of pairwise interactions within the solvent shell, taking advantage of the more favorable, compared to the case of OCS, solvent−solvent interactions in CO_2. On the other hand, the ring structure of $I_2^-(OCS)_5$, shown in Figure 3, accentuates the strength of the solvent−solute interactions and the fact that solvent is bound more strongly near the waist of I_2^- than near its ends.

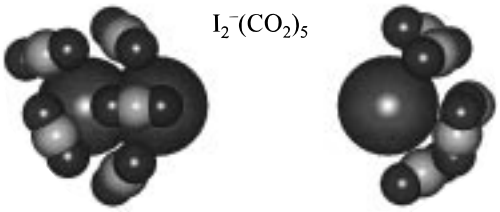

Figure 4. Calculated lowest-energy structure of $I_2^-(CO_2)_5$ as viewed along axes perpendicular (left) and parallel (right) to the I_2^- bond. Adapted from ref 11. Color version of this figure (Figure 4S) can be found on-line in the Supporting Information section of the Web edition of this publication.

III. Experimental Section

A detailed description of the ion beam apparatus has been given elsewhere.[82] The $I_2^-(OCS)_n$ cluster ions were formed by attachment of slow secondary electrons to neutral clusters in an electron-impact ionized supersonic jet, with subsequent nucleation around the negatively charged core.[34] The gas sample was prepared by passing a 5−7% OCS in Ar mixture through a reservoir containing crystalline iodine, heated to 50 °C to increase the iodine vapor pressure. The resulting gas mixture was expanded through a pulsed (30 Hz) supersonic valve at a stagnation pressure of 1.5 atm. A continuous electron beam (1 keV, ~700 μA) intersected the expansion 1−5 mm downstream from the valve orifice. The precursor ion mass selection was achieved in a Wiley−McLaren TOF mass spectrometer. The dominant ions in the primary beam were the $I_2^-(OCS)_n$ and $(OCS)_n^-$ clusters. The distribution of $I_2^-(OCS)_n$ clusters in the primary ion beam displays a single "magic number" corresponding to $I_2^-(OCS)_{11}$: this mass peak is typically a factor of 2 more intense than $I_2^-(OCS)_{10}$ and $I_2^-(OCS)_{12}$. No other noticeable discontinuities were observed over the cluster size range studied (n = 1−26). Metastable decay of the $I_2^-(OCS)_n$ cluster ions was not observed, and the parent ion internal temperature is believed to be similar to the ~50 K estimated[83] for $I_2^-(CO_2)_n$. At this temperature, I_2^- embedded in the cluster is predominantly in the ground vibrational state (115 cm^{-1} vibrational frequency), and the cluster can be considered solid.[38,84] Mass analysis of ionic fragments was carried out utilizing a second, reflectron mass spectrometer[85,86] tilted at a small angle with respect to the primary ion beam axis. The reflected ionic fragments were detected at the spatial focus of the reflectron with a microchannel plate (MCP) detector. The ion signal was amplified and sent to a transient digitizer for averaging and subsequent transfer to a computer. The precursor ion signal was simultaneously monitored with another MCP detector positioned directly behind the reflectron.

The fundamental or frequency-doubled output of a Quanta-Ray PDL-1 dye laser pumped with the second harmonic of a Quanta-Ray DCR-3 Nd:YAG laser was used as a source of the 790 and 395 nm radiation (<10 ns pulse duration; ~5 and 0.7 mJ/pulse at 790 and 395 nm, respectively). The fragment ion spectra correspond to those ionic fragments produced during the flight time from the photoabsorption region to the second mass spectrometer, ~10 μs. Fragmentation taking longer would not be detected. The fragment ion TOF mass spectra were

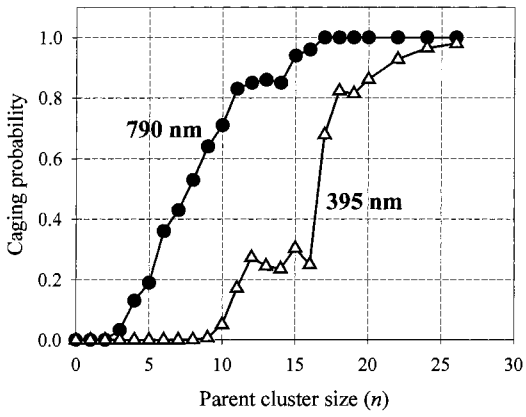

Figure 5. Probabilities of I_2^- recombination (caging) in $I_2^-(OCS)_n$ clusters following photoexcitation at 790 and 395 nm as functions of the parent cluster size.

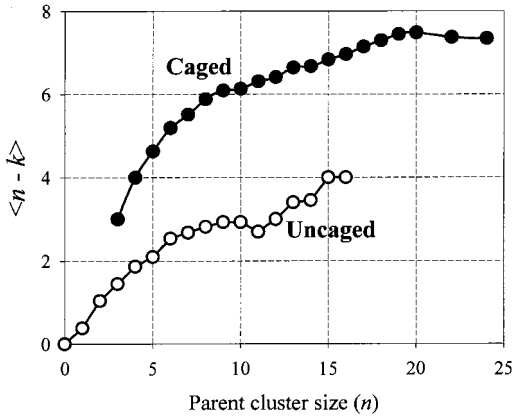

Figure 6. Average numbers of OCS solvent molecules lost in $I_2^-(OCS)_n$ photofragmentation via the caged and uncaged channels plotted as functions of the parent cluster size.

recorded by averaging between 3000 and 10 000 laser shots. Subsequently, the mass spectrum peaks were integrated, and the relative yields of different products were determined. Carbonyl sulfide and its neutral clusters are transparent at both 790 and 395 nm,[87−89] leaving I_2^- as the active chromophore in the $I_2^-(OCS)_n$ cluster ions at these wavelengths.

IV. Experimental Results

A. Near-IR (1.57 eV) Photofragmentation of $I_2^-(OCS)_n$ Cluster Ions. The photodissociation of $I_2^-(OCS)_n$ clusters leads (in general) to two types of ionic fragments: (1) "caged" $I_2^-(OCS)_k$ products and (2) "uncaged" $I^-(OCS)_k$ products. In both channels, the excess excitation energy is removed from the cluster by ejecting $(n - k)$ solvent OCS molecules.

In 790 nm photodissociation of I_2^-, only the $I^- + I(^2P_{3/2})$ dissociation channel is energetically accessible, corresponding to a translational energy release of 560 meV. The fraction of caged fragments observed in 790 nm photodissociation of $I_2^-(OCS)_n$ cluster ions is plotted in Figure 5 as a function of the parent cluster size n. No caged products are observed for parent clusters with $n < 3$. For larger $I_2^-(OCS)_n$ cluster ions, the caging fraction increases monotonically until reaching a plateau at $n = 11-14$, followed by a steplike increase at $n = 15$. Complete caging is observed for parent clusters with $n = 17$. The size (k) distributions of both types of 790 nm photoproducts {i.e., $I_2^-(OCS)_k$ and $I_2^-(OCS)_k$} are either bell-shaped (for larger parent clusters) or bell-shaped but truncated at $k = 0$ (for smaller parent clusters), consistent with participation of single energetic pathways in both the dissociation and recombination processes. The typical width of the k-distribution in both caged and uncaged product channels is fwhm $\approx$ 1.5−2.

The average number of solvent molecules lost by the cluster, $\langle n - k \rangle$, provides information about the sum of average solvent binding energy and translational energy release. This average is plotted in Figure 6 as a function of the parent cluster size. The curve corresponding to the caged channel levels off at ≈7.4 solvent molecules lost. Assuming that the recombination takes place on the ground state of I_2^-, this asymptotic value corresponds to the average number of the solvent molecules that must be ejected from the cluster in order to dissipate the energy of the photon (1.57 eV). From this value, we estimate that the loss of each solvent molecule stabilizes the cluster by ≈210 meV.

B. Near-UV (3.14 eV) Photofragmentation of $I_2^-(OCS)_n$ Cluster Ions. Excitation of the $B\ ^2\Sigma^+_{g,1/2} \leftarrow X\ ^2\Sigma^+_{u,1/2}$ transition

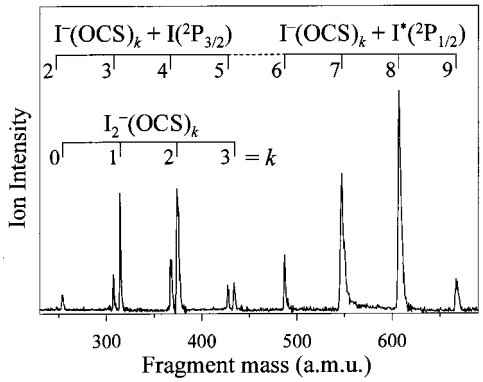

Figure 7. Representative ionic photofragment mass-spectrum obtained in 395 nm photodissociation of $I_2^-(OCS)_{12}$.

(see Figure 1) at 395 nm in bare I_2^- leads exclusively to dissociation on the spin−orbit excited $I^- + I^*(^2P_{1/2})$ asymptote with a translational energy release of 1.2 eV. Our measurement of the translational energy release did not reveal any 395 nm photodissociation products of I_2^- formed on the ground $I^- + I(^2P_{3/2})$ spin−orbit asymptote. However, in the presence of the solvent, dissociation on both $I^- + I(^2P_{1/2,3/2})$ spin−orbit asymptotes is observed for some cluster sizes. We also observe caging on the ground-state I_2^- potential energy surface, which must also be preceded by $I^* \rightarrow I$ relaxation. Thus, three classes of photofragments are observed in the near-UV photodissociation of $I_2^-(OCS)_n$: the uncaged $I^-(OCS)_k$ fragments formed on both $I^- + I(^2P_{1/2,3/2})$ spin−orbit asymptotes and the caged $I_2^-(OCS)_k$ products.

For example, Figure 7 shows the photofragment mass spectrum obtained following 395 nm photodissociation of $I_2^-(OCS)_{12}$. The existence of two uncaged pathways is manifest in the bimodal size (k) distribution of the $I^-(OCS)_k$ products, as compared to a single-mode distribution of the caged $I_2^-(OCS)_k$ fragments. A bimodal distribution is not observed for parent clusters with $n \leq 7$, for which the distribution of uncaged products is narrow, spanning a range of about three solvent molecules. For parent clusters with $n \geq 8$ the width of the uncaged product distribution increases gradually, until a bimodal distribution emerges at $n \approx 10$. The maxima of the two parts of the $I^-(OCS)_k$ product distribution are separated by $\Delta k \approx 4$, corresponding energetically to a ≈1 eV energy difference between the two uncaged channels, consistent with the 0.93 eV spin−orbit splitting in iodine. The larger-k $I^-(OCS)_k$ products are thus energetically consistent with dissociation on the upper spin−orbit asymptote, while the smaller

uncaged products result from dissociation on the ground spin−orbit asymptote. For $I_2^-(OCS)_{12}$ and larger parent clusters, the $I^- + I(^2P_{3/2})$ part of the bimodal distribution accounts, on average, for about 10% of the total uncaged product yield.

The fraction of caged fragments observed following 395 nm excitation is plotted in Figure 5 as a function of the parent cluster size *n*; it is compared with the corresponding curve for 790 nm excitation. The onset of 395 nm caging is observed at $n = 8$. Although complete caging is not achieved up to $n = 26$, the largest precursor studied {caging probability in $I_2^-(OCS)_{26}$ is 0.98}, recombination is the dominant reaction pathway for parent clusters with $n \geq 17$. A prominent feature of the 395 nm caging probability curve is the plateau at $n = 12-16$ followed by a steplike increase in caging at $n = 17$. Notably, $n = 17$ is the smallest parent cluster size for which 100% caging is observed at 790 nm.

V. Discussion

The loss of about seven solvent molecules in the 790 nm "caged" channel is energetically consistent with recombination on the ground electronic state of I_2^- followed by complete vibrational relaxation. The asymptotic value of $\langle n - k \rangle \approx 7.4$ (see Figure 6) obtained for large precursor clusters corresponds to ~210 meV of excess energy being removed from the cluster by each solvent molecule lost. Since the energy loss per solvent is a sum of the solvent binding energy to the cluster and the translational energy release, the above estimate is an upper bound of the average binding energy of OCS to large $I_2^-(OCS)_n$ clusters. For evaporative processes, calculations of Engelking[90] predict a kinetic release of 10−20% of the binding energy, corresponding to about 20−40 meV in the present case. Therefore, assuming an evaporative solvent loss mechanism, the average binding energy can be estimated at ~170−190 meV per OCS molecule.

This estimate is larger than the one derived from ab initio calculations (140 meV), but smaller than the 230 meV value obtained using the model Hamiltonian treatment (see section II). However, the above theoretical estimates were obtained for the binding of a single OCS molecule to I_2^- and may not be representative of the solvent binding energy to a large cluster. Moreover, the solvent loss energetics in the $I_2^-(OCS)_n$ clusters are strikingly similar to those observed for $I_2^-(CO_2)_n$ (upper bound of the solvent binding energy 250 meV), despite the structural differences between the two types of cluster ions, raising the possibility that a solvent loss mechanism differing from statistical evaporation may play a role. Time-resolved studies of transient dynamics in the OCS solvent cage indicated that nonstatistical solvent dynamics persist for >10 ps.[46] Impulsive ejection of solvent molecules during this nonstatistical epoch in the evolution of the excited cluster may result in an increased overall kinetic release to the solvent.

The theoretical simulations in section II indicate that 17 OCS molecules make up one complete solvent shell around I_2^-. This finding is consistent with several experimental observations. First, in the case of 790 nm photodissociation, 17 OCS molecules comprise the smallest solvent shell for which complete recombination of the chromophore is observed. Second, in the 395 nm photodissociation, the caging probability increases abruptly from 0.25 for $n = 16$ to 0.68 for $n = 17$. The sharp increase in 395 nm caging at $n = 17$ is preceded by a plateau between $n = 12$ and 16 (see Figure 5). Although less pronounced, this plateau is also apparent in 790 nm photodissociation. Thus, in the intermediate cluster size range additional OCS molecules do not result in a notably stronger solvent cage. The increase in caging upon addition of the 17th solvent molecule is probably due to a steric effect: as predicted in section II, the 17th molecule occupies the site at an end of I_2^-, closing the last collision-free escape route for the $I^- + I$ dissociation fragments. The presence of solvent on the I_2^- dissociation coordinate also increases the likelihood of nonadiabatic quenching of I*, a prerequisite for 395 nm caging.

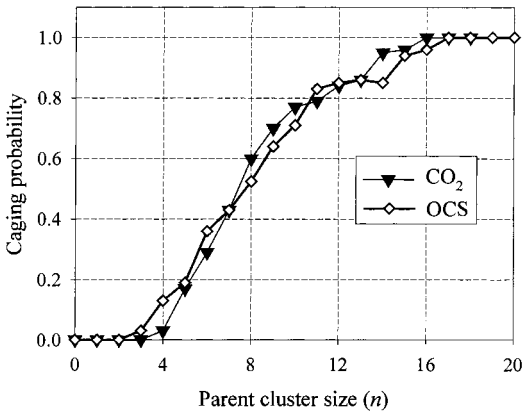

Figure 8. Comparison of I_2^- caging probabilities (plotted as functions of the parent cluster size) in the $I_2^-(CO_2)_n$ and $I_2^-(OCS)_n$ clusters following 790 nm photoexcitation.

One intriguing feature of the $I_2^-(OCS)_n$ cluster structures discussed in section II is the formation of five-membered solvent rings around the chromophore (see Figure 3). The first ring of five OCS molecules is formed around the waist of I_2^-, followed by a second ring closer to one of the ends of I_2^-. The 11th solvent molecule, "capping" one end of the cluster, then supplements the two rings. The arrangement of solvent in $I_2^-(OCS)_{11}$ (see Figure 3) can therefore be regarded as a half-solvent shell structure. The $I_2^-(OCS)_{11}$ cluster corresponds to a prominent "magic number" in the primary $I_2^-(OCS)_n$ mass spectrum, supporting the structure model discussed in section II. The buildup of the first solvent shell continues with the formation of the third five-membered solvent ring at the other end of I_2^-. Remarkably, the addition of the 12th OCS molecule to the half-shell structure of $I_2^-(OCS)_{11}$ appears to be unfavorable, since the $I_2^-(OCS)_{12}$ peak in the primary mass spectrum is typically about a factor of 2 less intense than $I_2^-(OCS)_{11}$. Since no "magic numbers" corresponding to the completion of individual five-membered solvent rings [i.e., $I_2^-(OCS)_5$, $I_2^-(OCS)_{10}$, and $I_2^-(OCS)_{16}$] could be discerned in the primary mass spectrum, these structures are apparently not significantly more stable than their neighbors.

Despite the different nature of the dominant solvent−solute and solvent−solvent interactions in the $I_2^-(OCS)_n$ and $I_2^-(CO_2)_n$ clusters, the 790 nm photofragmentation results are remarkably similar. For comparison, the 790 nm caging probabilities for $I_2^-(OCS)_n$ and $I_2^-(CO_2)_n$ are plotted in Figure 8. Complete 790 nm caging in $I_2^-(CO_2)_n$ is observed for $n = 16$.[91] This result is consistent with the first solvent shell closing at $n = 16-17$, as predicted by Monte Carlo simulations.[60,77,79,92] Similar to $I_2^-(OCS)_n$ but contrary to the $I_2^-Ar_n$ clusters,[29,38] molecular dynamics simulations revealed no recombination on the weakly bound first excited $A\ ^2\Pi_{g,3/2}$ state in $I_2^-(CO_2)_n$.[11] The onset of 790 nm caging in $I_2^-(OCS)_n$ at $n = 3$ leads to additional inferences about the OCS packing around the chromophore. Fewer OCS molecules are needed to retard the escaping fragments and induce caging than are required in the case of CO_2 (see Figure 8), perhaps due to the longer range of charge−dipole interactions in $I_2^-(OCS)_n$ compared to charge−quadrupole interactions in $I_2^-(CO_2)_n$.

The energy of 395 nm photons is above the adiabatic threshold (2.55 eV) for the electron detachment from I_2^-. While the electron photodetachment from $I_2^-(OCS)_n$ clusters (with $n > 2$) is energetically impossible due to additional stabilization of the anion by solvation, electron transfer to the solvent following 395 nm photoexcitation is energetically allowed. However, since no photochemistry characteristic of the negatively charged OCS clusters[63] has been observed, we conclude that the electron transfer does not occur. Possible reasons for the absence of the electron transfer are (1) the large amount of energy ($\sim$1 eV) required (in excess of the I_2^- photodetachment energy) to attach the electron to a *linear* OCS molecule; (2) significant solvent rearrangement required to accommodate electrostatic interaction with the relocated charge, also increasing the *vertical* excitation energy required for the electron transfer; and finally, (3) the absence of solvent pairs with the relative arrangement favoring the formation of covalently bound $(OCS)_2^-$ dimer anions which have been shown[63,64] to be the core of some $(OCS)_n^-$ cluster ions. The electron transfer to the solvent may be possible at higher excitation energies.

A new finding in this work is the detection of solvent-induced nonadiabatic spin−orbit quenching of iodine following 395 nm photodissociation of I_2^-. It results in the bimodal size distribution of uncaged fragments and the appearance of caged products. A bimodal distribution of uncaged products is clearly observed for parent $I_2^-(OCS)_n$ with $n \approx 10$ and larger, although both uncaged channels are probably present for smaller clusters as well, as intimated by the broadening of the uncaged product distribution starting from $n \approx 7$. The latter parent size approximately coincides with the observed onset of caging. Caging at 395 nm is a two-step process: nonadiabatic coupling to a lower $I\cdots I^-$ electronic state, correlating with the $I(^2P_{3/2}) + I^-$ dissociation asymptote (see Figure 1), followed by recombination and vibrational relaxation. While the observed percentage of uncaged fragments formed on the lower spin−orbit asymptote never exceeds 15% of the total yield of $I^-(OCS)_k$ products, a nearly 100% caging is observed for the largest parent clusters. For the largest $I_2^-(OCS)_n$ clusters studied at 395 nm the average caged product loses more than 13 solvent molecules, consistent with an asymptotic value of 7.4 solvent molecules lost following 790 nm photofragmentation, but suggests a somewhat larger solvent kinetic energy release.

The observation of a bimodal *k*-distribution of $I^-(OCS)_k$ products indicates that the spin−orbit relaxation of I* proceeds via a nonradiative mechanism, since the $\sim$1 eV of the spin−orbit excitation energy of iodine is removed from the cluster via the loss of additional solvent molecules. It is likely that the coupling between different $I\cdots I^-$ electronic states, leading to spin−orbit relaxation, takes place at large interatomic separations, where the solvent-induced perturbation of the electronic structure of I_2^- is expected to be most significant. We cannot completely rule out the possibility that the I_2^- − solvent interaction leads to 395 nm excitation of admixtures of electronic states correlating with both spin−orbit asymptotes, as a result of state mixing in the Franck−Condon region. However, since even at its maximum near 790 nm the excitation cross section of the I_2^- states correlating with the $I(^2P_{3/2})$ channel is much smaller than that of the 395 nm B ← X transition, the importance of state mixing in the near-UV excitation is expected to be negligible.

One possible mechanism for the solvent-induced spin−orbit relaxation is suggested by theoretical studies of the electronic structure of solvated I_2^- and nonadiabatic molecular-dynamics simulations of the photofragmentation and recombination dynamics.[9,44,60,93,94] In the isolated anion, the excess charge is shared equally between the two atoms. An asymmetric solvent environment polarizes the solute, causing the charge to localize preferentially on a single atom. The direction of this polarization is state-dependent, however. In the ground state and in the a′ and A states the charge tends to localize on the more solvated atom ("normal" charge flow), while in the B, A′, and a states the charge moves away from the solvent ("anomalous" charge flow).[11,38] As a result of the more favorable (shorter-range) electrostatic interaction of the excess charge with the solvent, "normal" states are shifted downward in energy by an asymmetric solvent environment, and this shift increases with increasing internuclear separation in I_2^-. In contrast, "anomalous" states are shifted to higher energy. The magnitude of these shifts can be a significant fraction of the solvation energy, $\sim$0.2 eV *per solvent molecule*. Therefore, the "normal" and "anomalous" states that are separated by an energy gap of $\sim$1 eV in the isolated molecule can become degenerate in the cluster of even a moderate size, providing a pathway for rapid nonadiabatic transitions.

Recent nonadiabatic molecular dynamics simulations[93] suggest that, following 395 nm excitation of the B ← X transition in I_2^-, the first step in the relaxation process is a nonadiabatic transition to the "normal" a′ state, followed by a solvent-induced transition to the "anomalous" A′ or a states correlating with the ground spin−orbit state of the I atom. This latter transition becomes nearly resonant within a cluster because the opposing solvation shifts between the two types of states compensate for the 1 eV gap between the ground and spin−orbit excited states of I. Alternatively, the electronic quenching may result from internal conversion within an $I(OCS)_m$ van der Waals complex. This mechanism is similar to the one proposed by McDonald et al. for the spin−orbit relaxation of $Br^*(^2P_{1/2})$ within the Br·I_2 complex, occurring on a time scale of $\sim$50 ps.[95,96]

VI. Conclusions

In summary, we reported the near-IR and near-UV photofragmentation of the $I_2^-(OCS)_n$ clusters. Following the photoexcitation of I_2^- via the near-IR absorption band, complete recombination (caging) of the chromophore is observed in clusters with $n = 17$. This is consistent with the theoretical prediction of the first complete solvent shell around I_2^- formed by 17 OCS molecules.

The photodissociation of $I_2^-(OCS)_n$ at 395 nm promotes the chromophore to an excited repulsive state correlating with the $I^- + I^*(^2P_{1/2})$ dissociation asymptote and results in three competing reaction pathways: (1) direct dissociation on the $I^- + I^*(^2P_{1/2})$ asymptote; (2) spin−orbit quenching of I* followed by dissociation on the $I^- + I(^2P_{3/2})$ asymptote, releasing nearly 1 eV more energy than the first pathway; (3) spin−orbit quenching of I* followed by the recombination of I_2^-, ultimately terminating on the ground electronic state. The existence of the two uncaged pathways is demonstrated by the bimodal size distribution of the $I^-(OCS)_k$ products. For smaller parent clusters ($n \leq 16$), pathway 1 is the dominant fragmentation channel. A sharp shift in the fragmentation pattern is observed between $n = 16$ and 17, where chromophore recombination, or caging, becomes the dominant reaction pathway. Since the cluster size where this change occurs corresponds to the predicted size of the first complete solvent shell around I_2^-, a likely interpretation is that the 17th OCS molecule "caps" the cluster, closing the last collisionless escape route for the dissociation fragment. This leads to an increased effectiveness of nonadiabatic coupling to the lower spin−orbit asymptote,

which is a prerequisite for caging. A remarkable result is that the caging and, therefore, the quenching probabilities approach unity in the largest clusters studied [e.g., $I_2^-(OCS)_{26}$].

Future experiments will investigate the dependence of spin−orbit relaxation on the nature of the solvent (for example, comparing OCS and CO_2). Ultrafast pump−probe experiments will elucidate the dynamical effects and time scales of this progress.

Acknowledgment. The authors thank Dr. D. W. Boo and Dr. M. Nadal for help in setting up the experiment and Dr. R. Loomis and T. Onasch for thorough reading of early drafts of this paper. Editorial help of Marilee DeGoede is greatly appreciated. This work is supported by the National Science Foundation (Grants CHE97-03486 and PHY95-12150), the Air Force Office of Scientific Research (AASERT program), and the National Center for Supercomputing Applications (NCSA, Grant CHE970015N for computing time on the Silicon Graphics Power ChallengeArray at the NCSA, University of Illinois at Urbana-Champaign).

Supporting Information Available: Table (in tab-delimited ASCII format) containing numerical data for the $I^-(OCS)$ potential energy surface shown in Figure 2 (file: PESdata.txt); color versions of Figures 2, 3, and 4 (Figures 2S, 3S, and 4S, respectively) (12 pages). Ordering information is given on any current masthead page.

References and Notes

(1) Troe, J. *Annu. Rev. Phys. Chem.* **1978**, *29*, 223.
(2) Otto, B.; Schroeder, J.; Troe, J. *J. Chem. Phys.* **1984**, *81*, 202.
(3) Kunz, H.; McCaffrey, J. G.; Schriever, R.; Schwentner, N. *J. Chem. Phys.* **1991**, *94*, 1039.
(4) Xu, J.; Schwentner, N.; Chergui, M. *J. Chem. Phys.* **1994**, *101*, 7381.
(5) Godderz, K. H.; Schwentner, N.; Chergui, M. *J. Chem. Phys.* **1996**, *105*, 451.
(6) Bondybey, V. E.; Brus, L. E. *Adv. Chem. Phys.* **1980**, *41*, 269.
(7) Dardi, P. S.; Dahler, J. S. *J. Chem. Phys.* **1990**, *93*, 242.
(8) Tripathi, G. N. R.; Schuler, R. H.; Fessenden, R. W. *Chem. Phys. Lett.* **1985**, *113*, 563.
(9) Batista, V. S.; Coker, D. F. *J. Chem. Phys.* **1997**, *106*, 7102.
(10) Ladanyi, B. M.; Parson, R. *J. Chem. Phys.* **1997**, *107*, 9326.
(11) Delaney, N.; Faeder, J.; Maslen, P. E.; Parson, R. *J. Phys. Chem. A* **1997**, *101*, 8147.
(12) Xu, X.; Yu, S.; Lingle, R.; Zhu, H.; Hopkins, J. B. *J. Chem. Phys.* **1991**, *95*, 2445.
(13) Harris, A. L.; Brown, J. K.; Harris, C. B. *Annu. Rev. Phys. Chem.* **1988**, *39*, 341.
(14) Zadoyan, R.; Li, Z.; Martens, C. C.; Apkarian, V. A. *J. Chem. Phys.* **1994**, *101*, 6648.
(15) Zadoyan, R.; Li, Z.; Ashjian, P.; Martens, C. C.; Apkarian, V. A. *Chem. Phys. Lett.* **1994**, *218*, 504.
(16) Liu, Q.; Wang, J. K.; Zewail, A. H. *Nature* **1993**, *364*, 427.
(17) Potter, E. D.; Liu, Q.; Zewail, A. H. *Chem. Phys. Lett.* **1992**, *200*, 605.
(18) Liu, Q. L.; Wang, J. K.; Zewail, A. H. *J. Phys. Chem.* **1995**, *99*, 11321.
(19) Wang, J. K.; Liu, Q. L.; Zewail, A. H. *J. Phys. Chem.* **1995**, *99*, 11309.
(20) Johnson, A. E.; Levinger, N. E.; Barbara, P. F. *J. Phys. Chem.* **1992**, *96*, 7841.
(21) Kliner, D. A. V.; Alfano, J. C.; Barbara, P. F. *J. Chem. Phys.* **1993**, *98*, 5375.
(22) Alfano, J. C.; Kimura, Y.; Walhout, P. K.; Barbara, P. F. *Chem. Phys.* **1993**, *175*, 147.
(23) Greenblatt, B. J.; Zanni, M. T.; Neumark, D. M. *Science* **1997**, *276*, 1675.
(24) Parson, R.; Faeder, J. *Science* **1997**, *276*, 1660.
(25) Greenblatt, B. J.; Zanni, M. T.; Neumark, D. M. *Chem. Phys. Lett.* **1996**, *258*, 523.
(26) Papanikolas, J. M.; Vorsa, V.; Nadal, M. E.; Campagnola, P. J.; Buchenau, H. K.; Lineberger, W. C. *J. Chem. Phys.* **1993**, *99*, 8733.
(27) Papanikolas, J. M.; Vorsa, V.; Nadal, M. E.; Campagnola, P. J.; Gord, J. R.; Lineberger, W. C. *J. Chem. Phys.* **1992**, *97*, 7002.
(28) Vorsa, V.; Nandi, S.; Campagnola, P. J.; Larsson, M.; Lineberger, W. C. *J. Chem. Phys.* **1997**, *106*, 1402.
(29) Vorsa, V.; Campagnola, P. J.; Nandi, S.; Larsson, M.; Lineberger, W. C. *J. Chem. Phys.* **1996**, *105*, 2298.
(30) (a) Nadal, M. E. Ph.D. Thesis, University of Colorado, 1996. (b) Nadal, M. E.; Nandi, S.; Boo, D. W.; Lineberger, W. C., manuscript in preparation.
(31) Papanikolas, J. M.; Campagnola, P. J.; Vorsa, V.; Nadal, M. E.; Buchenau, H. K.; Parson, R.; Lineberger, W. C. Time-Resolved Studies of Cage Recombination Dynamics in Ionic Clusters. In *The Chemical Dynamics and Kinetics of Small Radicals*; Liu, K., Wagner, A., Eds.; World Scientific Publishing Co.: Singapore, 1995; Vol. 6, p 616.
(32) Papanikolas, J. M.; Gord, J. R.; Levinger, N. E.; Ray, D.; Vorsa, V.; Lineberger, W. C. *J. Phys. Chem.* **1991**, *95*, 8028.
(33) Ray, D.; Levinger, N. E.; Papanikolas, J. M.; Lineberger, W. C. *J. Chem. Phys.* **1989**, *91*, 6533.
(34) Johnson, M. A.; Lineberger, W. C. Pulsed Methods for Cluster Ion Spectroscopy. In *Techniques for the Study of Ion Molecule Reactions*; Farrar, J. M., Saunders, J. W., Eds.; Wiley: New York, 1988; p 591.
(35) Castleman, A. W.; Bowen, K. H. *J. Phys. Chem.* **1996**, *100*, 12911.
(36) Farrar, J. M. In *Current Topics in Ion Chemistry and Physics*; Ng, C. Y., Powis, I., Eds.; Wiley: New York, 1992.
(37) Castleman, A. W., Jr. In *Clusters of Atoms and Molecules*; Haberland, H., Ed.; Springer-Verlag: New York, 1992.
(38) Faeder, J.; Delaney, N.; Maslen, P. E.; Parson, R. *Chem. Phys. Lett.* **1997**, *270*, 196.
(39) Zanni, M. T.; Taylor, T. R.; Greenblatt, B. J.; Soep, B.; Neumark, D. M. *J. Chem. Phys.* **1997**, *107*, 7613.
(40) Maslen, P. E.; Faeder, J.; Parson, R. *Chem. Phys. Lett.* **1996**, *263*, 63.
(41) Dojahn, J. G.; Chen, E. C. M.; Wentworth, W. E. *J. Phys. Chem.* **1996**, *100*, 9649.
(42) Chen, E. C. M.; Wentworth, W. E. J. *J. Phys. Chem.* **1985**, *89*, 4099.
(43) Greenblatt, B. J.; Zanni, M. T.; Neumark, D. M. *Chem. Phys. Lett.* **1996**, *258*, 523.
(44) Maslen, P. E.; Papanikolas, J. M.; Faeder, J.; Parson, R.; O'Neil, S. V. *J. Chem. Phys.* **1994**, *101*, 5731.
(45) Lineberger, W. C.; Nadal, M. E.; Campagnola, P. J.; Vorsa, V.; Kleiber, P. D.; Papanikolas, J. M.; Maslen, P. E.; Faeder, J.; Parson, R.; Poplawski, O. Time-Resolved Dynamics in Large Cluster Ions. In *Proceedings of The Robert A. Welch Foundation 38th Conference on Chemical Research: Chemical Dynamics of Transient Species, 1994, Houston, TX*.
(46) Sanov, A.; Nandi, S.; Lineberger, W. C. *J. Chem. Phys.* **1998**, *108*, 5155.
(47) Sanov, A.; Lineberger, W. C. *Proc. SPIE* **1998**, *3271*, 188.
(48) Yasumatsu, H.; Kalmbach, U.; Koizumi, S.; Terasaki, A.; Kondow, T. *Z. Phys. D* **1997**, *40*, 1.
(49) Yasumatsu, H.; Terasaki, A.; Kondow, T. *J. Chem. Phys.* **1997**, *106*, 3806.
(50) Yasumatsu, H.; Koizumi, S.; Terasaki, A.; Kondow, T. *J. Chem. Phys.* **1996**, *105*, 9509.
(51) Yasumatsu, H.; Tsukuda, T.; Sugai, T.; Terasaki, A.; Nagata, T.; Kondow, T. *Surf. Rev. Lett.* **1996**, *3*, 901.
(52) Benjamin, I.; Barbara, P. F.; Gertner, B. J.; Hynes, J. T. *J. Phys. Chem.* **1995**, *99*, 7557.
(53) Bianco, R.; Hynes, J. T. *J. Chem. Phys.* **1995**, *102*, 7885.
(54) Faeder, J.; Delaney, N.; Maslen, P. E.; Parson, R. *J. Phys. Chem. A*, in press.
(55) Albery, W. J. *Annu. Rev. Phys. Chem.* **1980**, *31*, 227.
(56) Marcus, R. A. *J. Chem. Phys.* **1956**, *24*, 966.
(57) Shide, T.; Takahashi, Y.; Hatano, H. *Chem. Phys. Lett.* **1975**, *33*, 491.
(58) Delbecq, C. J.; Hayes, W.; Yuster, P. H. *Phys. Rev.* **1961**, *121*, 1043.
(59) Buckingham, A. D.; Disch, R. L.; Dunmur, D. A. *J. Am. Chem. Soc.* **1968**, *90*, 3104.
(60) Papanikolas, J. M.; Maslen, P. E.; Parson, R. *J. Chem. Phys.* **1995**, *102*, 2452.
(61) Battaglia, M. R.; Buckingham, A. D.; Neumark, D.; Pierens, R. K.; Williams, J. H. *Mol. Phys.* **1981**, *43*, 1015.
(62) Buckingham, A. D.; Graham, C.; Williams, J. H. *Mol. Phys.* **1988**, *49*, 703.
(63) Sanov, A.; Nandi, S.; Jordan, K. D.; Lineberger, W. C. *J. Chem. Phys.* **1998**, *109*, 1264.
(64) Sanov, A.; Lineberger, W. C.; Jordan, K. D., manuscript in preparation.
(65) Bone, R. G. A. *Chem. Phys. Lett.* **1993**, *206*, 260.
(66) Frisch, M. J.; Trucks, G. W.; Schlegal, H. B.; Gill, P. M. W.; Johnson, B. G.; Robb, M. A.; Cheeseman, J. R.; Kieth, T.; Petersson, G. A.; Montgomery, J. A.; Raghavachari, K.; Al-Laham, M. A.; Zakrewski, V. G.; Ortiz, J. V.; Foresman, J. B.; Cioslowski, J.; Stefanov, B. B.; Nanayakkara, A.; Challacombe, M.; Peng, C. Y.; Ayala, P. Y.; Chen, W.;

Wong, M. W.; Andres, J. L.; Replogle, E. S.; Gomperts, R.; Martin, R. L.; Fox, D. J.; Binkley, J. S.; Defrees, D. J.; Baker, J.; Stewart, J. P.; Head-Gordon, M.; Gonzalez, C.; Pople, J. A. *Gaussian 94, Rev. E.1*; Gaussian, Inc.: Pittsburgh, PA, 1995.

(67) Becke, A. D. *J. Chem. Phys.* **1993**, *98*, 5648.

(68) Lee, C.; Yang, W.; Parr, R. G. *Phys. Rev. B* **1988**, *37*, 785.

(69) Wadt, W. R.; Hay, P. J. *J. Chem. Phys.* **1985**, *82*, 284.

(70) Glukhovtsev, M. N.; Pross, A.; Radom, L. *J. Am. Chem. Soc.* **1995**, *117*, 2024.

(71) Dunning Jr., T. H. *J. Chem. Phys.* **1989**, *90*, 1007.

(72) Kendall, R. A.; Dunning Jr., T. H.; Harrison, R. J. *J. Chem. Phys.* **1992**, *96*, 6796.

(73) Woon, D. E.; Dunning Jr., T. H. *J. Chem. Phys.* **1993**, *98*, 1358.

(74) Arnold, D. W.; Bradforth, S. E.; Kim, E. H.; Neumark, D. M. *J. Chem. Phys.* **1995**, *102*, 3510.

(75) Arnold, D. W.; Bradforth, S. E.; Kim, E. H.; Neumark, D. M. *J. Chem. Phys.* **1995**, *102*, 3493.

(76) Sanov, A.; Lineberger, W. C., unpublished results.

(77) Faeder, J.; Delaney, N.; Maslen, P. E.; Parson, R. *Chem. Phys.*, submitted for publication.

(78) Maslen, P. E.; Faeder, J.; Parson, R. *Mol. Phys.*, in press.

(79) Faeder, J. Ph.D. Thesis, University of Colorado, 1998.

(80) Gray, C. G.; Gubbins, K. E. *Theory of Molecular Fluids*; Clarendon Press: Oxford, 1984; Vol. 1: Fundamentals.

(81) Samions, J.; Stassen, H.; Dorfmuller, T. *Chem. Phys.* **1992**, *160*, 33.

(82) Nadal, M. E.; Kleiber, P. D.; Lineberger, W. C. *J. Chem. Phys.* **1996**, *105*, 504.

(83) Levinger, N. E. University of Colorado at Boulder, 1990.

(84) Davis, H. L.; Jellinek, J.; Berry, R. S. *J. Chem. Phys.* **1987**, *86*, 6456.

(85) Alexander, M. L. Ph.D. Thesis, University of Colorado, 1987.

(86) Mamyrin, B. A.; Karataev, V. I.; Shmikk, D. V.; Zagulin, V. A. *Sov. Phys.-JEPT* **1973**, *37*, 45.

(87) Ono, Y.; Osuch, E. A.; Ng, C. Y. *J. Chem. Phys.* **1981**, *74*, 1645.

(88) Fayt, A.; Vandenhaute, R.; Lahaye, J. G. *J. Mol. Spectrosc.* **1986**, *119*, 233.

(89) Breckenridge, W. H.; Taube, H. *J. Chem. Phys.* **1970**, *52*, 1713.

(90) Engelking, P. C. *J. Chem. Phys.* **1987**, *87*, 936.

(91) Vorsa, V. Ph.D. Thesis, University of Colorado, 1996.

(92) Papanikolas, J. M. Ph.D. Thesis, University of Colorado, 1994.

(93) Delaney, N.; Faeder, J.; Parson, R., manuscript in preparation.

(94) Coker, D. F.; Xiao, L. *J. Chem. Phys.* **1995**, *102*, 496.

(95) Tuchler, M. F.; Wright, S.; McDonald, J. D. *J. Chem. Phys.* **1997**, *106*, 2634.

(96) Wright, S. A.; Tuchler, M. F.; McDonald, J. D. *Chem. Phys. Lett.* **1994**, *226*, 5.